Journal of Catalysis 275 (2010) 129–139

Contents lists available at ScienceDirect

Journal of Catalysis

journal homepage: www.elsevier.com/locate/jcat

Highly selective hydrogenation of butadiene on Pt/Sn alloy elucidated by first-principles calculations

F. Vigné [a], J. Haubrich [b], D. Loffreda [a], P. Sautet [a], F. Delbecq [a,*]

[a] Université de Lyon, Institut de Chimie, Laboratoire de Chimie, Ecole Normale Supérieure de Lyon and CNRS, 46 allée d'Italie, 69364 Lyon Cedex 07, France
[b] Institut für Physikalische und Theoretische Chemie der Universität Bonn, Wegelerstr. 12, 53115 Bonn, Germany

ARTICLE INFO

Article history:
Received 19 March 2010
Revised 12 July 2010
Accepted 22 July 2010
Available online 21 August 2010

Keywords:
Butadiene
Butene
Hydrogenation
Platinum
Tin
Alloy
DFT calculations
Selectivity

ABSTRACT

Reaction pathways have been explored with periodic DFT calculations in order to understand the origin of the high selectivity for the hydrogenation of 1,3-butadiene on the Pt_2Sn/Pt(1 1 1)-($\sqrt{3} \times \sqrt{3}$)R30° surface alloy. The adsorption structures of butadiene, 1- and 2-butenes and all the intermediate species have been studied. Compared to the reference catalyst Pt(1 1 1), there is a change both in geometries and in relative energies: for instance, the best adsorption mode of butadiene is *cis* 1,4-di-σ-2,3-π, while it is *trans* 1,2,3,4-tetra-σ on Pt(1 1 1). On the alloy, all the adsorption energies are reduced compared to pure platinum, and the adsorption structures implying many Pt—C bonds are more destabilized. The different pathways leading to partial hydrogenation products (1-butene, 2-butene) or other intermediate surface species (1,3- and 1,4-metallacycles) have been explored. The first hydrogenation step is clearly preferred at a terminal carbon, and the further hydrogenation to 1-butene has by far the lowest barrier. Other pathways exhibit larger activation barriers, particularly those leading to metallacycles, which is the key to explain the high selectivity to butene, in contrast to Pt(1 1 1). The role of tin is dual: a role of site blocking that forces unselective pathways to adopt distorted, high-energy transition states and a role of ligand that weakens the molecular adsorption and allows decoordination of double bonds prior to the hydrogenation, which decreases the energy barriers for the selective pathway to butene.

1. Introduction

The selective hydrogenation of dienes into mono-olefins is an important industrial process for the purification of the alkene streams used in polymerization. Group VIII metals like platinum or palladium have been used for a long time as hydrogenation catalysts for this reaction. Most of the studies are devoted to the partial hydrogenation of the simplest diene, 1,3-butadiene, into butene. In order to elucidate the origin of the selectivity (formation of butene rather than butane), many experimental studies have been carried out for two decades on the adsorption and hydrogenation of butadiene and butene on metallic single crystals [1–7] or on metal particles dispersed on silica or alumina [8–11]. The following conclusions arose from these various works: Pd is almost totally selective in butene, whereas Pt leads to a mixture of butene and butane, the latter being partly formed as primary product of the reaction. Depending on the experimental conditions and on the percentage of conversion, the selectivity to butenes is in the range 65–87%, with about 70–80% of 1-butene and 30–20% of 2-butenes. The most commonly admitted interpretation of this different behavior rests on the different competitive adsorption energies of butadiene and butene on the two metals. To verify this assumption, the adsorption structures of 1,3-butadiene and of butenes (1- and 2-butene) have been investigated by theoretical calculations [12–14]. In the two latter papers, the difference between the adsorption energies of butadiene and butenes has been found very similar on Pt and Pd and hence it cannot account for the observed selectivity. Moreover, the formation of butane as a primary product cannot be explained by considering only reaction thermodynamics.

To solve this question, a theoretical study of the hydrogenation mechanism on Pt and Pd has been tackled recently [15]. In this work, the role of dihydrogenated C_4H_8 metallacycle intermediate species, obtained by 1-3 or 2-3 hydrogenation, is underlined. These species cannot desorb from the surface and can evolve to butane by hydrogenation. The activation barriers for the formation of such species are high on Pd(1 1 1) and they cannot compete with the formation of butene. Conversely on Pt(1 1 1), their formation is as probable as that of butene, which explains the lower selectivity toward this compound and the formation of butane as a primary product.

To enhance the selectivity toward butene, other types of catalysts have been tested, namely alloys of platinum or palladium. It is well known that alloying these metals with another one deeply modifies their catalytic properties. Tin is often used as second metal. For example, one can cite PdSn particles deposited on alumina

* Corresponding author. Fax: +33 4 72 72 88 60.
E-mail address: francoise.delbecq@ens-lyon.fr (F. Delbecq).

0021-9517/$ - see front matter © 2010 Elsevier Inc. All rights reserved.
doi:10.1016/j.jcat.2010.07.019

[16,17], the (1 1 1) surface of the Pt_3Sn alloy [18] or ordered Pt_xSn/Pt(1 1 1) surface alloys [19]. These model catalysts are less active than the pure metal but more selective toward butene. In the case of the Pt/Sn alloys, the selectivity to butenes ranges from 98% to 100%, with about 80% of 1-butene. The same behavior has also been found for the Pd/Au alloy [20]. These results raise the question of the role of the second metal in the selectivity enhancement.

In order to answer this question, we have explored the pathways for butadiene hydrogenation on the Pt/Sn surface alloys, more precisely on Pt_2Sn/Pt(1 1 1)-($\sqrt{3} \times \sqrt{3}$)R30° on the basis of density functional theory (DFT) calculations. In the present paper, we first report on the adsorption structures of butadiene, 1- and 2-butenes, and hydrogen on this surface. In a second part, we address the mechanism of the butadiene partial hydrogenation and compare it with the one found for Pt(1 1 1) and Pd(1 1 1). More particularly, we compare the formation of the various C_4H_8 species that we have shown to be the key of the selectivity on these two metals.

2. Computational details

The calculations were performed in the framework of the density functional theory (DFT) using the Vienna *Ab Initio* Simulation Program (VASP) [21–23]. The one-electron functions are developed on a basis of plane waves. The electron–ion interactions were described by the projector-augmented wave method (PAW) introduced by Blöchl [24] and adapted by Kresse and Joubert [25]. A tight convergence of the plane-wave expansion was obtained with a cutoff of 400 eV. The exchange–correlation energy and potential were described by the generalized gradient approximation (Perdew–Wang 91) [26].

The surface alloy was modeled by a periodic four-layer slab, where only the first layer contains Sn atoms in a stoichiometry Pt_2Sn. Indeed, by Sn vapor deposition on Pt(1 1 1) followed by annealing, two structures are formed depending on the amount of Sn, namely (2×2) with stoichiometry Pt_3Sn and ($\sqrt{3} \times \sqrt{3}$)R30° with stoichiometry Pt_2Sn [27]. XPD data have shown that these compounds are two-dimensional surface alloys [28]. Each slab is separated from its periodic image in the *z* direction by a sufficiently large vacuum space corresponding to five layers (11.5 Å). 3×3 supercells containing nine atoms per layer are used (see Fig. 1). The 2D Brillouin zone integrations have been performed on a $3 \times 3 \times 1$ Monkhorst–Pack grid since it was found to be accurate as well as computationally efficient for this cell size. The Pt–Pt distance optimized from Pt bulk calculations (2.82 Å) has been used for the frozen part of the slab. This is justified by the fact that experimentally the lattice parameter is imposed by the underlying Pt bulk, and the Sn atoms in the uppermost layer accommodate this constraint by an outward displacement, inducing a Pt–Sn distance of 2.86 Å.

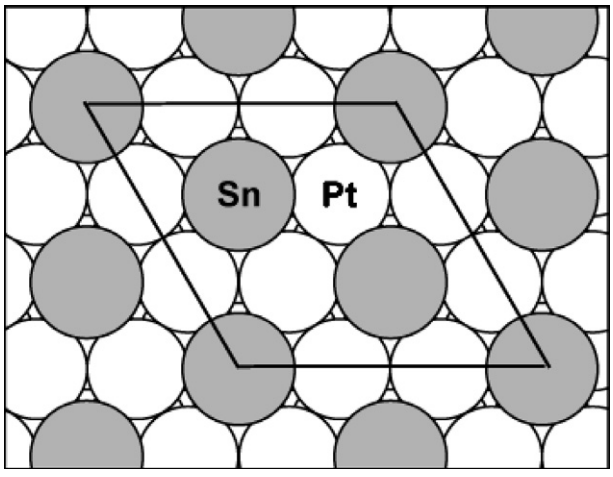

Fig. 1. Top view of the ($\sqrt{3} \times \sqrt{3}$)R30° Pt_2Sn/Pt(1 1 1) surface alloy. Platinum and tin are colored in white and gray, respectively. The subsurface layers only contain platinum. The diamond represents the 3×3 unit cell.

Adsorption and reaction were performed on one side of the metal slab with one molecule adsorbed per unit cell, which gives a coverage $\theta = 1/9$. The geometries of the two uppermost layers of the surface together with the adsorbate (C_4H_x , $x = 6$–8 species) were fully optimized, whereas the two lowest metal planes were kept fixed. The adsorption modes and the corresponding adsorption energies for all the C_4H_x moieties were determined. The reaction intermediates were studied on different adsorption sites. For sake of simplicity, only the most stable structures are reported here. Coadsorption with hydrogen has also been explored in detail by comparing various possible situations.

The energy along the reaction (E_{react}) was calculated using butadiene and H_2 in the gas phase as the energy reference with the following expression:

$$E_{react} = E_{syst/surface} - E_{surface} - E_{C_4H_{6(g)}} - E_{H_{2(g)}}$$

A negative value indicates an exothermic chemisorption process. The system is a C_4H_x species and $(8 - x)$ hydrogen atoms ($x = 6$, 7, 8) adsorbed on the surface. If we consider that the hydrogen atoms and the hydrocarbon do not initially interact, the $E_{syst/surface}$ term is then obtained by combining the results from independent slab calculations for the molecular species and the hydrogen atoms:

$$E_{syst/surface} = E_{C_4H_x/surface} + (8 - x)(E_{H/surface} - E_{surface})$$

In order to directly compare with previous results, the adsorption energy for the species existing in the gas phase has also been reported ($E_{ads} = E_{C_4H_x/surface} - E_{surface} - E_{C_4H_x}$). The energies of the transition states (E_{TS}) were calculated with respect to adsorbed butadiene and two adsorbed hydrogen atoms without interaction.

In order to obtain more detailed insights into the changes of adsorption energy, it is decomposed in deformation energy and interaction energy terms following the equation:

$$E_{ads} = E_{Int} + E_{Def,Mol} + E_{Def,Surf}$$

where $E_{Def,Mol}$ and $E_{Def,Surf}$ are the deformation energies of the molecule and of the surface, respectively, calculated as the difference between the energies of the optimized geometry of the considered moiety and of the geometry it has in the adsorbed system. E_{Int} is the interaction energy between the two moieties in their deformed geometry.

The Nudged Elastic Band method (NEB), developed by Jónsson and coworkers [29], has been used to determine the transition states, with sets of 8 or 16 intermediate images along the reaction pathways. The obtained approximate transition states have been refined by minimizing residual forces below 0.01 eV/Å with the *quasi*-Newton algorithm implemented in VASP. To validate the saddle points, a vibrational analysis including adsorbate and relaxed substrate degrees of freedom has been performed. The presence of a single imaginary frequency (negative force constant) and the consistency of the corresponding normal mode with the reaction path have been checked.

The prediction of atomistic thermodynamics in reaction conditions is crucial here. A simple way to estimate the stability of the reactant and the products on the catalytic surface is the prediction of the Gibbs free adsorption energy ΔG_{ads}, according to the following formula (see [30] and references therein for the elaboration of the corresponding model):

$$\Delta G_{ads} = G_{ads} - G_{surf} - G_{gas} \quad (1)$$

$$G = PV - Nk_BT - Nk_BT\ln\left(\frac{Q}{N}\right) \quad (2)$$

$$\Delta G_{ads}(T,P) = \frac{1}{A}\left(\Delta E_{ads} + \Delta E_{ZPE} + F_{config,ads} - Nk_BT - Nk_BT\ln\left(\frac{Q^{vib}_{ads}(T)Q^{trans}_{ads}(T)}{Q^{vib}_{gas}(T)Q^{rot}_{gas}(T)Q^{trans}_{gas}(T,P)}\right)\right) \quad (3)$$

$$F_{config,ads} = -k_BT\ln Q_{config,ads} = -k_BT\ln\left(\frac{N_{site}!}{(N_{site}-N_{ads})!N_{ads}!}\right) \quad (4)$$

where ΔE_{ads} and ΔE_{ZPE} are the DFT adsorption energy and the DFT zero point energy change due to adsorption, respectively, Q^{vib}_{ads} and Q^{vib}_{gas} being the respective vibrational partition functions of the adsorbed system and the gas phase (excluding the metal phonons), Q^{trans}_{ads} and Q^{trans}_{gas} being the respective translational partition functions of the adsorbed system and the gas phase and Q^{rot}_{gas} being the rotational partition function of the gas phase. $F_{config,ads}$ is the configurational free energy of the adsorbed phase. A is the unit area of the considered supercell.

3. Adsorption of the species involved in the mechanism, C_4H_x (x = 6–8) and H

Scheme 1 summarizes the different steps for the dihydrogenation of 1,3-butadiene. The first hydrogen can attack at C^1 or C^2 giving either 3-buten-1-yl or 1-buten-3-yl, respectively, adsorbed on the surface. These species can be further hydrogenated at three possible positions giving either 1-butene or 2-butene that can desorb in the gas phase or butan-1,3 and 1,4-diyls that remain adsorbed on the surface and can evolve to butane by further hydrogenations. The study of the adsorption structures and corresponding energies of all these species is a prerequisite to the investigation into the reactivity and selectivity. The molecules existing in the gas phase are first explored.

3.1. Adsorption of 1,3-butadiene and butenes on Pt_2Sn/Pt(1 1 1)

A large number of adsorption geometries have been considered for 1,3-butadiene on the surface alloy. We have previously noticed that the binding of the carbon atoms to tin atoms is not favored [31]. Hence, the presence of tin reduces the number of adsorption possibilities and favors some conformations over others. As a result, the *trans* 1,2,3,4-tetra-σ structure that is the most stable on Pt(1 1 1) and Pd(1 1 1) does not exist anymore on the Pt_2Sn/Pt(1 1 1) alloy, since the necessary ensemble of 4 Pt atoms is not found on the Pt_2Sn/Pt(1 1 1). The most stable adsorbed structure on the alloy is *cis* 1,4-di-σ-2,3-π, as it can be seen in Table 1, followed by *trans* 1,2-π-3,4-π. Two other structures have also favorable adsorption energies, *trans* 1,2-π-3,4-di-σ and *cis* 1,2-π-3,4-π, although 20 kJ mol^{-1} less stable. The structures where the molecule is bound by only one double bond are significantly less stable (40 kJ mol^{-1}), with nevertheless a smaller difference than on Pt(1 1 1) (60 kJ mol^{-1}). The various optimized adsorption geometries are shown in Fig. 2.

Hence, the most stable conformation of butadiene on Pt_2Sn/Pt(1 1 1) is the *cis* one (by 11 kJ mol^{-1}), whereas in the gas phase, it is the trans one (by 17 kJ mol^{-1}). However, the inter-conversion is associated with a low barrier. In gas phase, this barrier is 31 kJ mol^{-1}. On the surface, a complex multistep low-energy pathway was found. From the *trans* 1,2-π-3,4-π structure, the molecule first moves to the *trans* 1,2-π-3,4-di-σ geometry with a barrier of 40 kJ mol^{-1} (see Fig. 2). Then, the C^1—C^2 double bond decoordinates and the *trans* 3,4-di-σ form is obtained with a barrier of 30 kJ mol^{-1}. The rotation around C^2—C^3 occurs at this stage with a barrier of 26 kJ mol^{-1}, giving the *cis* 3,4-di-σ structure. Finally, the most stable *cis* 1,4-di-σ-2,3-π form is obtained by a rotation of the molecule and the recoordination of the C^1—C^2 double bond with almost no barrier (3 kJ mol^{-1}). Hence, in gas phase or on the surface, *trans–cis* isomerization is fast, and hence the butadiene structures will quickly equilibrate to a predominant most stable *cis* 1,4-di-σ-2,3-π structure, which has been selected as the starting point for the hydrogenation pathway exploration.

For 1- and 2-butenes, the two possible adsorption geometries (di-σ and π) have also been compared. There is a change in the relative order of this two geometries compared to Pt(1 1 1): on the alloy, the π form becomes as stable as the di-σ one, and even more stable in the case of 2-butene. All these results are also collected in Table 1, and the structures are shown in Fig. 3.

For all the species, the Pt—C bond lengths are in the same range as those found on Pt(1 1 1) (2.13–2.23 Å) [14] except for the *trans* 1,2-π-3,4-di-σ structure, where a long Pt—C^2 bond is found. The

Table 1
Adsorption energies (E_{ads}, kJ mol^{-1}) for the most stable chemisorption structures of 1,3-butadiene, 1-butene and *cis*/*trans* 2-butenes on Pt_2Sn/Pt(1 1 1) and relevant bond lengths (Å). Available adsorption energies on Pt(1 1 1) (E_{ads}/Pt) with a similar approach are also given.

	E_{ads}	Pt—C^1	Pt—C^2	Pt—C^3	Pt—C^4	C^1—C^2	C^2—C^3	C^3—C^4	E_{ads}/Pt
1,3-butadiene									
cis 1,4-di-σ-2,3-π	−74	2.14	2.27	2.25	2.13	1.47	1.43	1.48	−150
trans 1,2-π-3,4-π	−63	2.17	2.23	2.23	2.20	1.41	1.47	1.41	−122
trans 1,2-π-3,4-di-σ	−55	2.17	2.44	2.19	2.14	1.42	1.46	1.49	
cis 1,2-π-3,4-π	−53	2.18	2.25	2.24	2.16	1.42	1.48	1.42	−116
trans 3,4-di-σ	−35	–	–	2.17	2.13	1.34	1.47	1.49	−89
trans 3,4-π	−32			2.27	2.17	1.34	1.46	1.42	
cis 3,4-di-σ	−31	–	–	2.18	2.13	1.35	1.48	1.49	
cis 1,4-di-σ	−27	2.17	–	–	2.17	1.46	1.38	1.46	
cis 3,4-π	−26			2.25	2.18	1.34	1.47	1.41	
trans 1,4-di-σ	−8	2.16	–	–	2.18	1.47	1.38	1.47	
1-butene									
di-σ	−49	–	–	2.15	2.14	1.54	1.52	1.49	−101
π	−48	–	–	2.19	2.23	1.54	1.51	1.41	−70
cis 2-butene									
di-σ	−21	–	2.15	2.15	–	1.52	1.50	1.52	−81
π	−27	–	2.22	2.23	–	1.50	1.42	1.50	−59
trans 2-butene									
di-σ	−27	–	2.14	2.13	–	1.52	1.50	1.52	−81
π	−25	–	2.22	2.20	–	1.51	1.42	1.50	−49

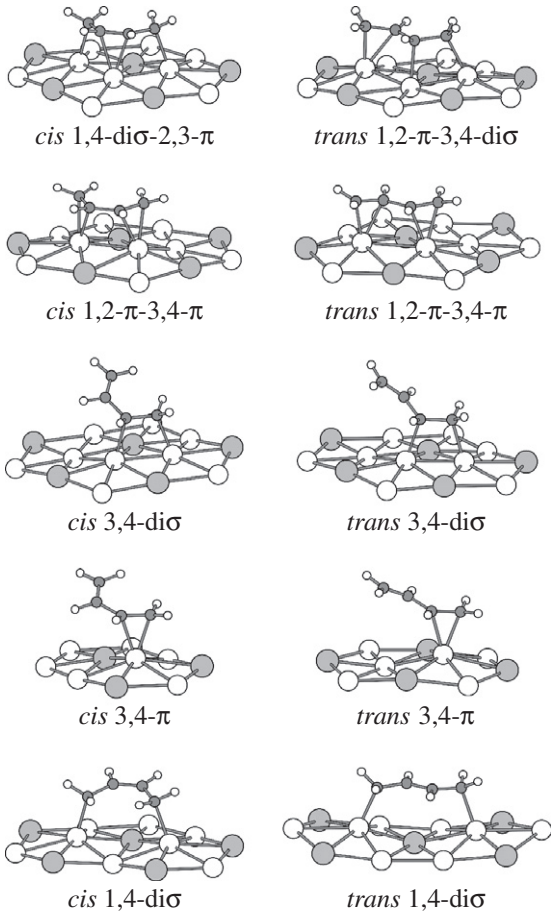

Fig. 2. Optimized adsorption structures of 1,3-butadiene on ($\sqrt{3} \times \sqrt{3}$)R30° Pt_2Sn/Pt(1 1 1).

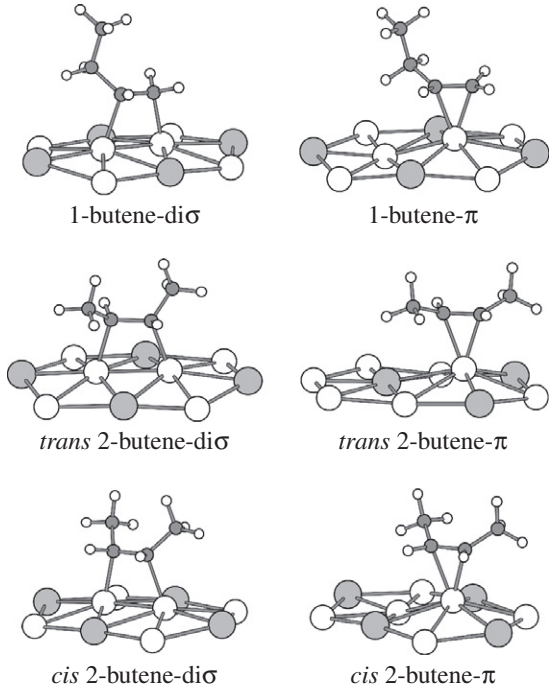

Fig. 3. Optimized adsorption structures of 1-butene and 2-butene on ($\sqrt{3} \times \sqrt{3}$)R30° Pt_2Sn/Pt(1 1 1).

C—C bonds involved in the adsorption have the characteristic lengths for a di-σ adsorption (1.47–1.53 Å) or a π adsorption (1.41–1.43 Å), the difference being explained by a stronger hybridization toward sp^3 in the case of the di-σ adsorption type. Compared to the values previously found on Pt(1 1 1) [14], the adsorption energies on Pt_2Sn/Pt(1 1 1) are much smaller. A decrease of 76 kJ mol^{-1} is observed for butadiene (74 vs. 150 kJ mol^{-1} for the *cis* 1,4-di-σ-2,3-π form), of 52 kJ mol^{-1} for 1-butene and of 51 kJ mol^{-1} for 2-butene. The calculated adsorption energies of butadiene and 1-butene on Pt_2Sn/Pt(1 1 1) (74 and 49 kJ mol^{-1}) are in very good agreement with the values deduced from TPD experiments (75 and 54 kJ mol^{-1}, respectively) [32,33]. Such a decrease in the adsorption energy of alkenes on the Pt/Sn alloys compared to pure Pt has been observed experimentally [33] and has been explained by DFT calculations [31,34,35]. The occupied d-band center is lower below the Fermi level for Pt2Sn (−2.57 eV) than for Pt (−2.39 eV) [35]. This results in a smaller interaction with the π system of the adsorbed molecules. Moreover, an electronic transfer occurs from Sn to Pt, and the surface Pt atoms are more negatively charged on the alloy, which induces larger Pauli repulsions.

An interesting feature on the alloy is the similarity between the adsorption energies of the di-σ and the π structures in the case of the butene molecules, whereas these energies are very different on pure platinum. For the *cis* 2-butene, the π form is even more stable than the di-σ one. An explanation can be derived from the decomposition of the adsorption energy into deformation energy and interaction energy. Results for this decomposition are given in Table 2. At first glance, it is obvious that the di-σ geometries are more deformed than the π ones and that the *trans* 2-butene is more deformed than the cis 2-butene. Such a decomposition has already been performed on Pt(1 1 1) for the two isomers of 2-butene [36]. The given explanation rests on the fact that cis 2-butene can more easily accommodate on the surface than *trans* 2-butene which has to distort much. When compared to Pt(1 1 1), the total deformation energy is globally higher on the alloy, the increase being larger for the di-σ forms than for the π ones. This is essentially due to the surface deformation, as it was already pointed out that the Pt/Sn alloy surface deforms more than that of Pt(1 1 1) upon alkene adsorption [37]. It results that the adsorption energy of the π forms is less decreased than that of the di-σ forms when Pt is alloyed with Sn. This change in the relative stability of the di-σ and π forms on the alloy explains the large decrease of the adsorption energy of butadiene on the alloy compared to pure platinum and the change in the relative stability order of the structures.

3.2. Stability diagram in operating conditions

The next step in the analysis is the prediction of the stability of these adsorbates in the operating conditions. Model reactivity

Table 2
Energy decomposition analysis for the adsorption of 1- and 2-butene on Pt(1 1 1) and Pt_2Sn/Pt(1 1 1). Deformation energies of the molecule $E_{Def,Mol}$ and of the surface $E_{Def,Surf}$ and interaction energy E_{Int} in kJ mol^{-1}.

	Pt(1 1 1)			Pt_2Sn/Pt(1 1 1)		
	$E_{Def,Mol}$	$E_{Def,Surf}$	E_{Int}	$E_{Def,Mol}$	$E_{Def,Surf}$	E_{Int}
1-butene						
di-σ	161	53	−315	151	68	−268
π	43	59	−172	34	61	−143
cis 2-butene						
di-σ	156	55	−292	162	76	−264
π	48	63	−170	49	70	−150
trans 2-butene						
di-σ	192	55	−328	202	72	−301
π	66	67	−182	61	74	−160

experiments on $Pt_2Sn/Pt(1\,1\,1)$ single-crystal surfaces were performed at 360 K for a total pressure of reactant of 15 Torr [18]. The Gibbs free adsorption energy diagrams of 1,3-butadiene, 1-butene, and *cis* and *trans* 2-butene have been plotted in Fig. 4 for $Pt(1\,1\,1)$ and $Pt_2Sn/Pt(1\,1\,1)$ at fixed pressure or fixed temperature.

In each case, only the most stable adsorption structure has been considered. On $Pt(1\,1\,1)$, the reactant and the first hydrogenation products are adsorbed on the catalyst around 360 K and at 15 Torr, the butenes being far less strongly adsorbed than butadiene. For a larger partial pressure of 1 atm, our results for butadiene and 1-butene differ significantly from those published previously in terms of desorption temperature [13]. This results from the different choice of the coverage (lower coverage in our case). More importantly, the implementation of the vibrational entropic contributions for both the adsorbed and the gas phases is essential to predict these diagrams according to our more complete thermodynamic model. On the alloy, the systematic marked weakening of the adsorption significantly shifts the stability domains to lower temperature regions. The major consequence is a weak adsorption for butadiene in the 360 K region and a spontaneous desorption of the butenes from the surface alloy, without possible further hydrogenation, as soon as these products are formed during the reaction. This thermodynamic result is one argument in favor of a high selectivity to butenes on the alloy. However, this explanation is only valid if the partial hydrogenation selectively forms butene by 1-2 or 1-4 hydrogenation and not metallacycle intermediates by 1-3 or 2-3 hydrogenation. These strongly bound metallacycles would yield butane as a primary product as on $Pt(1\,1\,1)$ [15]. Hence, in order to resolve this point, we have explored the possible hydrogenation pathways on the alloy.

3.3. Adsorbed structures of the radical (C_4H_7) and diradical (C_4H_8) species on $Pt_2Sn/Pt(1\,1\,1)$

Since we will only focus in the present study on the *cis* conformation of 1,3-butadiene for studying the reactivity, all the derived species will have the *cis* configuration. Fig. 5 shows the adsorption structures of the radicals obtained after the first and the second hydrogenation. 1-buten-3-yl and 3-buten-1-yl are adsorbed through three carbons giving a π-σ and a tri-σ arrangement, respectively. The butan-1,3 and 1,4-diyl diradicals are bound to the surface by two carbon atoms forming five-member and six-member metallacycles, respectively. The Pt—C and C—C bond lengths of all these species are given in Table 2. The Pt—C bonds

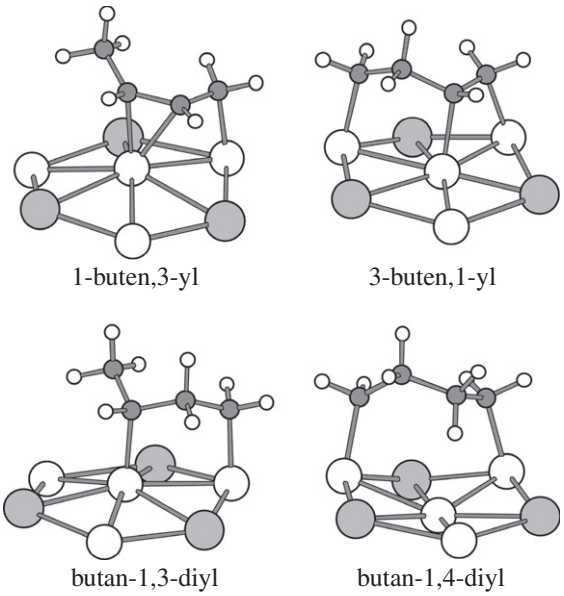

Fig. 5. Optimized adsorption geometries of the species obtained by the first and the second hydrogenation of 1,3-butadiene on $(\sqrt{3} \times \sqrt{3})R30°$ $Pt_2Sn/Pt(1\,1\,1)$.

are in the same range as before (2.12–2.21 Å) with only an exception for 1-buten-3-yl (2.27 Å). The C^3—C^4 bond length in 3-buten-1-yl corresponds to a strong di-σ adsorption type (1.50 Å). 1-buten-3-yl presents an allylic arrangement and the C^2—C^3 and C^3—C^4 bond lengths are rather similar (1.42 and 1.47 Å).

In order to compare the relative stability of all the species involved in the study, the reaction energies, which are calculated following the formulae given in Section 2, have been collected in Table 3. Like in the case of pure Pt, the allylic 1-buten-3-yl radical is more stable than the 3-buten-1-yl radical. However, contrary to the case of pure Pt, the hydrogenation reaction is exothermic on the alloy. Indeed, we have noticed previously that 1,3-butadiene, being bound to the surface by four bonds, is far more destabilized by the presence of tin than the butene molecules, only adsorbed through two bonds. If we consider the stability of the metallacycle structures, butan-1,4-diyl is 70–80 kJ mol^{-1} less stable than the butenes, and its formation is hence unlikely. In contrast, butan-1,3-diyl is only 10–20 kJ mol^{-1} less stable than the butenes, and

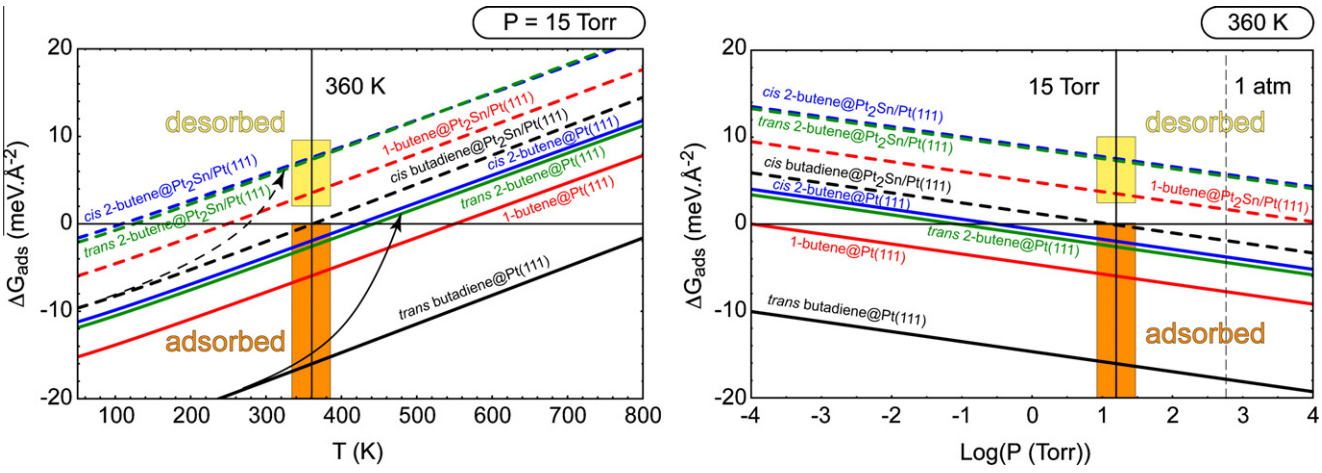

Fig. 4. Gibbs free adsorption energy diagrams (meV $Å^{-2}$) at a constant pressure (15 Torr) and at a constant temperature (360 K) for the reactant (butadiene) and the first hydrogenation products (1-butene, *cis* and *trans* 2-butene) on the $Pt(1\,1\,1)$ and $Pt_2Sn/Pt(1\,1\,1)$ surfaces. The coverage is associated with the (3×3) unit cell. A negative (positive) ΔG_{ads} means adsorption (desorption).

Table 3
Energies along the reaction (E_{react}, kJ mol^{-1}) and main bond lengths (in Å) for the C_4H_x (x = 6–8) species adsorbed on Pt_2Sn/Pt(1 1 1) involved in the reaction path. All species have the *cis* configuration.

	E_{react}	Pt—C^1	Pt—C^2	Pt—C^3	Pt—C^4	C^1-C^2	C^2—C^3	C^3—C^4
1,3-butadiene η_4	−134	2.14	2.27	2.25	2.13	1.47	1.43	1.48
1,3-butadiene η_2	−84			2.18	2.13	1.35	1.48	1.49
3-buten-1-yl	−122	2.11		2.14	2.14	1.53	1.53	1.50
1-buten-3-yl	−159		2.21	2.27	2.12	1.51	1.42	1.47
1-butene diσ	−166			2.15	2.13	1.52	1.53	1.50
1-butene π	−167			2.23	2.19	1.54	1.51	1.41
cis 2-butene π	−177		2.22	2.22		1.50	1.42	1.50
butan-1,4-diyl	−98	2.12			2.13	1.53	1.54	1.54
butan-1,3-diyl	−156		2.12		2.10	1.52	1.53	1.52
I_1	−133				2.13	1.49	1.35	1.47
I_2	−122				2.13	1.49	1.35	1.46
I_3	−98		2.15			1.52	1.48	1.35
TS_3	−82	3.38	2.83	2.19	2.13	1.35	1.47	1.49
TS_{10}	−127				2.12	1.49	1.36	1.47
TS_{11}	−105				2.12	1.49	1.35	1.47

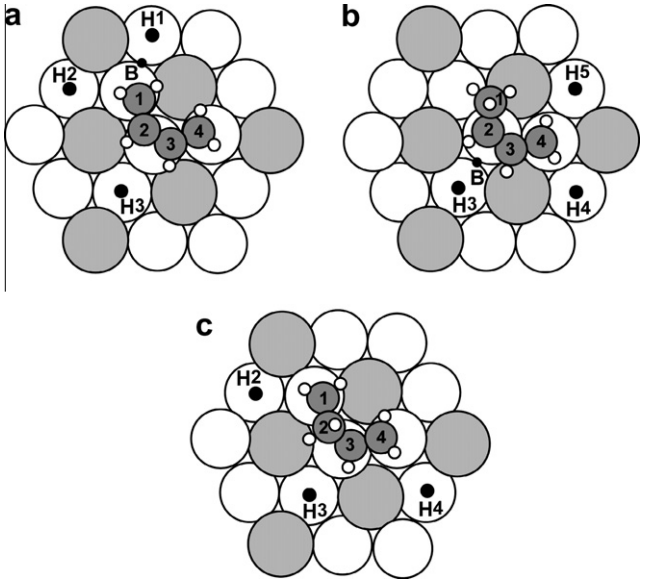

Fig. 6. Positions of the hydrogen atom in the coadsorption states with (a) 1,3-butadiene; (b) 1-buten-3-yl; (c) 3-buten-1-yl, starting points for the considered hydrogenation pathways.

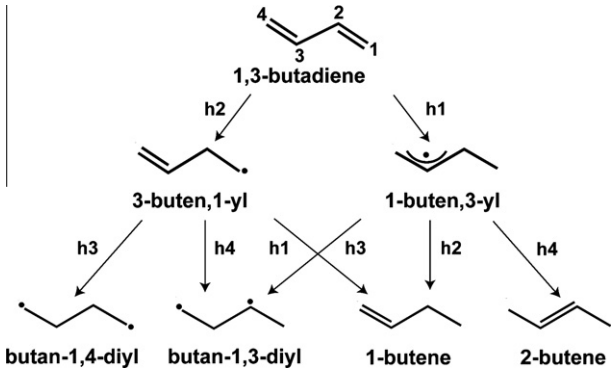

Scheme 1. Various steps for 1,3-butadiene hydrogenation to C_4H_8 species.

its presence on the surface cannot be excluded from the single thermodynamic argument.

3.4. Adsorption of hydrogen on Pt_2Sn/Pt(1 1 1) and coadsorption with C_4H_x species

The hydrogenation of the various C_4H_x species following a Horiuti–Polanyi-type mechanism requires the presence of coadsorbed hydrogen atoms on the surface. The possible adsorption sites for H atom have been compared: two apical sites, one atop a Pt atom and one atop a Sn atom (Scheme 2), one bridge site Pt–Pt and the two hollow sites (hcp and fcc) formed by two Pt and one Sn atoms. The site atop a Sn atom is not stable (99 kJ mol^{-1} less stable than the atop Pt one), and the hollow sites evolve to the bridge Pt–Pt site, with a binding energy of 11 kJ mol^{-1} relatively to 1/2 $H_{2(g)}$. The most stable site is apical atop a Pt atom with a binding energy of 30 kJ mol^{-1} relatively to 1/2 $H_{2(g)}$. The H atoms are less strongly adsorbed on Pt_2Sn than on Pt and are not on the same site since, on Pt(1 1 1), the best adsorption site is the hollow hcp one with an energy of 50 kJ mol^{-1}, the top site being only slightly less stable (45 kJ mol^{-1}). Hence, hydrogen, like carbon, does not bind to Sn atoms. These results are at variance with those obtained by Fearon et al. who found the Pt–Pt bridge site more stable than the atop Pt one [38].

The next step is the study of the coadsorption of the C_4H_x species with hydrogen. The C_4H_x species have been considered in their most stable adsorption site, and hydrogen has been placed at atop Pt sites close to the C atom to be hydrogenated. Several atop Pt positions around each species have been compared, and the most stable have been chosen as initial for the search of the reaction pathways. The various positions of the hydrogen atom around butadiene, 1-buten-3-yl and 3-buten-1-yl are shown in Fig. 6. The coadsorption induces a small destabilization not exceeding 0.1 eV, compared to the species adsorbed at infinite distance from each other.

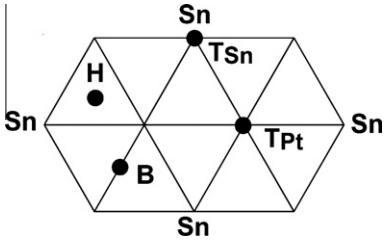

Scheme 2. Adsorption sites for atomic hydrogen on the Pt_2Sn/Pt(1 1 1) surface alloy. T_{Sn} and T_{Pt}: atop Sn and Pt atoms, respectively; B: bridge between two Pt atoms; H: threefold hollow site, either hcp or fcc.

4. Reaction pathways

Starting from the previously described coadsorption systems, the various hydrogenation steps shown in Scheme 1 have been explored and the corresponding transition states (TS) determined. For each TS, the three important bond lengths, C—H, Pt—H and Pt—C, are reported in Table 4 along with the TS energy relative to the system formed by 1,3-butadiene and two hydrogen atoms adsorbed at infinite distance (without any interaction) in their most stable positions.

Following Scheme 1, the first hydrogenation step can occur at C^2, leading to 3-buten-1-yl or at C^1 forming 1-buten-3-yl. The starting point for the hydrogenation at C^2 is H^3 (Fig. 6). It is evident that the approach of hydrogen is hindered by the tin atom. The transition state TS_1, shown in Fig. 7, looks like those already described for hydrogenation of acrolein [39] or butadiene on Pt(1 1 1) and Pd(1 1 1) [15]: the three atoms Pt, C^2 and H form a three-member ring TS. However, the particular case here is that C^3 is adsorbed on the same platinum atom than H, which leads to a Pt atom with too many ligands. This is the reason of the high activation barrier (136 kJ mol^{-1}, see Table 4).

The starting point for the hydrogenation at C^1 is either H^1 or H^2 (see Fig. 6). In each case, H can reach C^1 without coming too close to Sn. Whatever the starting point, the same TS is found (TS_2) after having passed through a hardly marked bridge intermediate (B in Fig. 6). TS_2 is also depicted in Fig. 7. The comparison of TS_1 and TS_2 from Table 4 shows that TS_2 is earlier than TS_1 with shorter Pt—H and Pt—C bonds and a longer C—H bond, which is related to the lower barrier (92 kJ mol^{-1}).

Besides this classical mechanism, a second pathway exists where the double bond to be hydrogenated decoordinates first, leading to a di-σ initial structure called butadiene η_2, corresponding to the *cis* 3,4-di-σ form of butadiene (Fig. 2) coadsorbed with H. This structure is 50 kJ mol^{-1} less stable than the η_4 form corresponding to the *cis* 1,4-di-σ-2,3-π form of butadiene (Fig. 2) coadsorbed with H (see Fig. 8). The transition state for this decoordination step (TS_3) in only 2 kJ mol^{-1} above η_2 butadiene and has a close geometry (compare Figs. 2 and 7 and Tables 1 and 3). Then, the hydrogenation proceeds with a small barrier of 21 kJ mol^{-1} through TS_4. This pathway has hence the lowest overall barrier, 71 kJ mol^{-1}. The TS structure is a six-center member ring (Fig. 7), in contrast to the usual three-center hydrogenation transition states. The occurrence of such a TS has been recently commented [40]. Attack at C^2 leading to 3-buten-1-yl has also been tested starting from butadiene η_2. However, hydrogenation at C^2 does not occur on the decoordinated C=C bond because of high strain in the molecule since C^1 needs to bind on the surface. The pathway leads to a recoordination to butadiene η_4 and then follows the path already described.

Starting from 3-buten-1-yl, three different attacks of a second H atom are possible, leading to 1-butene, butan-1,3-diyl and butan-1,4-diyl (Scheme 1) from positions H^2, H^4 and H^3, respectively (Fig. 6). The three pathways are single steps and the TS (TS_5, TS_6 and TS_7) are close in energy, within 11 kJ mol^{-1}. Their activation energies between 88 and 99 kJ mol^{-1} are in the same range as the ones found on Pt and Pd [15] and also in the case of the C=C bond hydrogenation in acrolein [39]. These TS are represented in Fig. 7 and described in Table 4. TS_5 is reactant-like with short Pt—H and Pt—C bonds and a long C—H bond. TS_6 and TS_7 are more products-like with slightly longer Pt—H and Pt—C bonds and a shorter C—H bond.

Starting from 1-buten-3-yl, three different pathways are also possible, leading to 1-butene, 2-butene and butan-1,3-diyl from positions H^3, H^4 or H^5 and H^3, respectively (see Fig. 6). Both paths leading to 2-butene from H^4 and H^5 are single steps. The corresponding barriers differ by 4 kJ mol^{-1} and only the path starting from H^4 will be described further. The transition state (TS_8) has intermediate bond lengths compared to TS_1–TS_2 and TS_5–TS_7, which gives a not too high barrier (70 kJ mol^{-1}). The path leading to butan-1,3-diyl can also be considered as a single step although a shallow bridge intermediate (B in Fig. 6) has been found, as in the case of TS_2. The associated transition state (TS_9) is more product-like and is associated with a energy of 92 kJ mol^{-1}. The path leading to 1-butene is more complicated since it presents three steps. First, the hydrogen atom remains in position H^3 and the organic species changes its adsorption mode from η_3 to η_1: carbon atoms C^2 and C^3 decoordinate so that only C^4 is bound to the surface and a free double bond is restored between C^2 and C^3 (see Fig. 9). This is reflected in the short C^2—C^3 bond, as shown in Table 2 for intermediate I_1. The second step consists in the migration of H to a second atop position nearer the organic species that keeps the same structure (see Fig. 9). This second intermediate I_2 has bond lengths very similar to those of I_1 (Table 3). The transition state TS_{10} between the starting point and I_1 represents the decoordination of the two carbon atoms and requires 29 kJ mol^{-1}. The second transition state TS_{11} corresponds to the H migration between two atop sites and needs 28 kJ mol^{-1}. Finally, the hydrogenation step only requires 21 kJ mol^{-1} (TS_{12}). The three transition states are also depicted in Fig. 7. Distances are not given in Table 3 for TS_{10} and TS_{11} because they are not hydrogenation transition states. In TS_{11}, the hydrogen atom is in a real atop position with a short Pt—H bond (1.58 Å) and the organic moiety has a geometry close to that of intermediate I_1. It differs by a longer C^2—C^3 bond, which indicates that the double bond is not totally formed, and by a shorter bond between C^3 and the Pt atom (3.0 Å in TS_{10} compared to 3.63 Å in I_1). The geometry difference between TS_{11} and I_2 comes only from the position of the H atom that lies between two Pt atoms in TS_{11}. Finally, the transition state for hydrogenation,

Table 4
Energies (E_{TS}, E_{react}(TS) kJ mol^{-1}), relevant bond lengths (Å) and imaginary frequencies (cm^{-1}) of the transition states for the 1,3-butadiene hydrogenation on Pt_2Sn/Pt(1 1 1). For E_{TS}, the energy reference is the system formed by adsorbed butadiene and two hydrogen atoms without interaction.

Transition state	E_{TS}	E_{react}(TS)	Pt—H	C—H	Pt—C	ν
butadiene → 3-buten-1-yl TS_1	136	2	1.69	1.47	2.34	907i
butadiene → 1-buten-3-yl TS_2	92	−42	1.61	1.57	2.32	780i
butadiene η_4 → butadiene η_2 TS_3	52	−82				53i
butadiene η_2 → 1-buten-3-yl TS_4	71	−63	1.64	1.74	2.78	288i
3-buten-1-yl → 1-butene TS_5	88	−46	1.58	1.69	2.27	636i
3-buten-1-yl → butan-1,3-diyl TS_6	92	−42	1.60	1.58	2.32	783i
3-buten-1-yl → butan-1,4-diyl TS_7	100	−34	1.60	1.58	2.36	794i
1-buten-3-yl → 2-butene TS_8	70	−64	1.64	1.56	2.32	921i
1-buten-3-yl → butan-1,3-diyl TS_9	92	−42	1.69	1.47	2.28	830i
1-buten-3-yl → I_1 TS_{10}	7	−127				33i
I_1 → I_2 TS_{11}	29	−105				459i
I_2 → 1-butene TS_{12}	33	−101	1.68	1.60		432i
I_3 → 2-butene TS_{13}	50	−84	1.66	1.68	2.81	337i

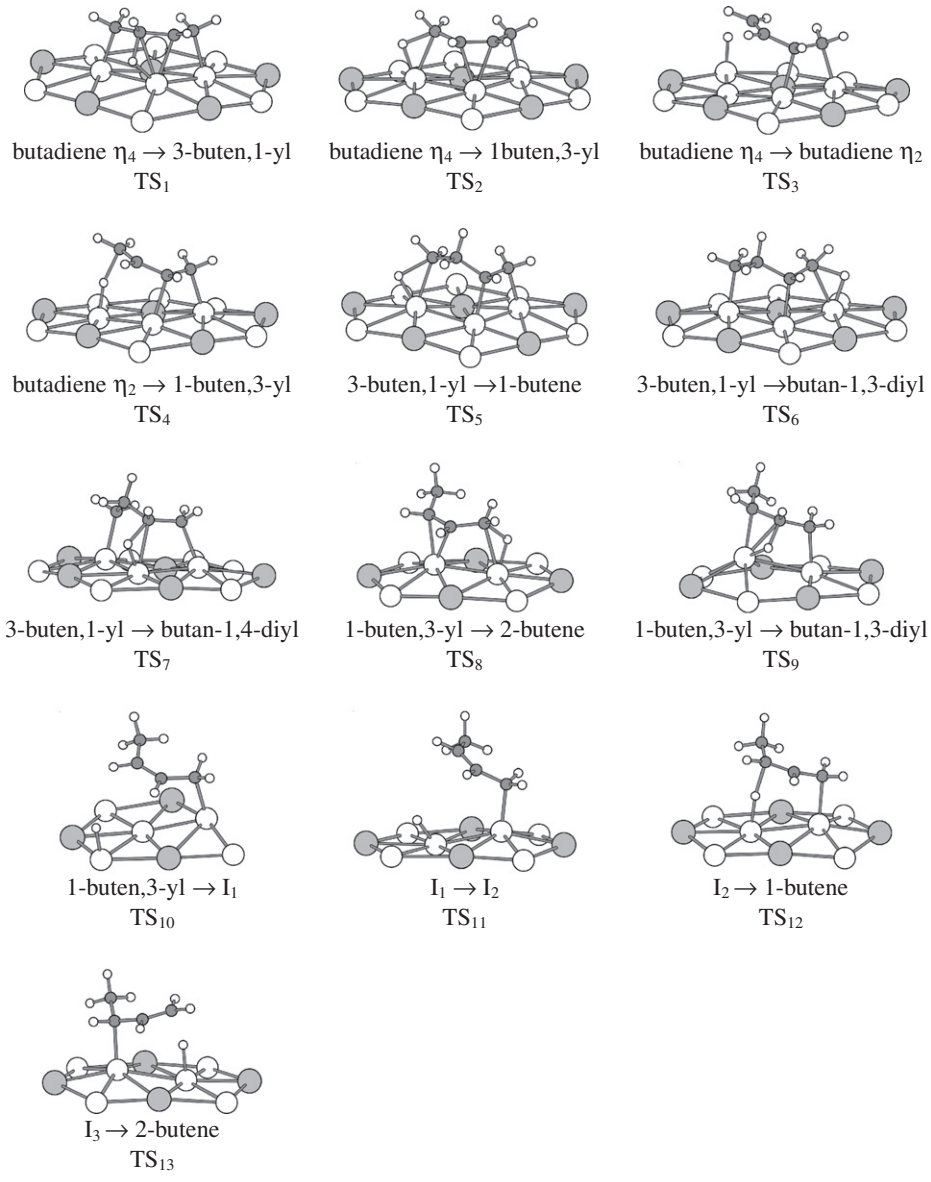

Fig. 7. Optimized structures of the transition states for all the elementary steps involved in the hydrogenation of 1,3-butadiene on $(\sqrt{3} \times \sqrt{3})R30°$ $Pt_2Sn/Pt(1\,1\,1)$.

TS_{12}, has both a long Pt—H and a long C—H bond. It must be specified that 1-butene is obtained here in the π adsorbed geometry, which avoids the presence of a Pt—C bond and a Pt—H bond on the same platinum atom. This path leading from 1-buten-3-yl to 1-butene illustrates again the existence of a six-member ring TS where the decoordination of the double bond occurs prior to its hydrogenation [40].

The hydrogenation at carbon C^3 of intermediate I_2 can also lead to butan-1,3-diyl. However, this pathway is disfavored by ca. 40 kJ mol^{-1} compared to the initial pathway occurring through TS_9. This is due to the difficult recoordination of C^2, like in the case of the hydrogenation of butadiene-η_2 leading to 3-buten-1-yl. In these two cases, the prior decoordination of the double bond is not a favorable pathway.

Finally, 1-buten-3-yl can also adsorb on the surface through C^2, regenerating a double bond between C^3 and C^4. This species is called I_3 and is depicted on Fig. 9. The corresponding distances are given in Table 3. It is 55 kJ mol^{-1} less stable than 1-buten-3-yl adsorbed in a η_3 geometry. The hydrogenation at carbon C^4 leading to 2-butene through TS_{13} only requires 15 kJ mol^{-1}. TS_{13} is described in Fig. 7 and Table 4. It is 20 kJ mol^{-1} more stable than TS_8, showing the advantage of the prior decoordination in this case.

The comparison of the imaginary frequencies in Table 4 shows that those corresponding to the hydrogenation of a decoordinated double bond are smaller, which indicates softer modes along the C—H bond formation process.

Fig. 8 summarizes the competitive reaction pathways starting from butadiene and coadsorbed hydrogen to give the partial hydrogenation products (C_4H_8), namely 1-butene, 2-butene and metallacycles butan-1,3 and 1,4-diyl. The energy reference is the energy of adsorbed 1,3-butadiene and two adsorbed hydrogen atoms at infinite distances (without interaction). The pathway passing through the formation of 3-buten-1-yl is represented at the top of Fig. 8 and the one passing through the formation of 1-buten-3-yl is represented at the bottom. The difference between the two paths is obvious. In the former, the first step leading to 3-buten-1-yl by attack at carbon C^2 is highly activated (136 kJ mol^{-1}) compared to that leading to 1-buten-3-yl by attack at the terminal carbon C^1 (71 kJ mol^{-1}). Then, the three transition states leading to butan-1,4-diyl, butan-1,3-diyl and 1-butene are close in energy so

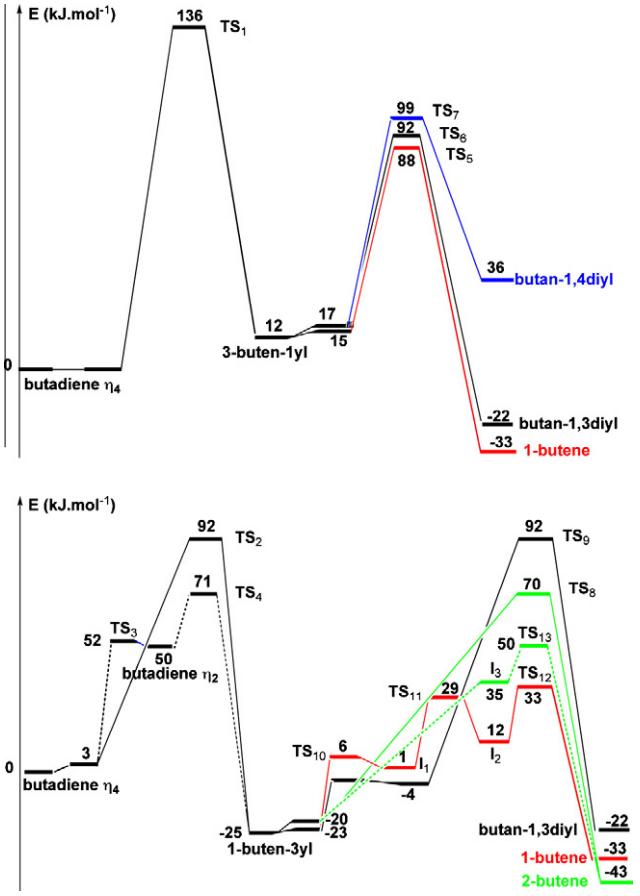

Fig. 8. Butadiene hydrogenation energy profiles on ($\sqrt{3} \times \sqrt{3}$)R30° Pt_2Sn/Pt(1 1 1) via 3-buten-1-yl (on top) and 1-buten-3-yl (bottom). The energy reference is the energy of butadiene coadsorbed with two hydrogen atoms at infinite distance.

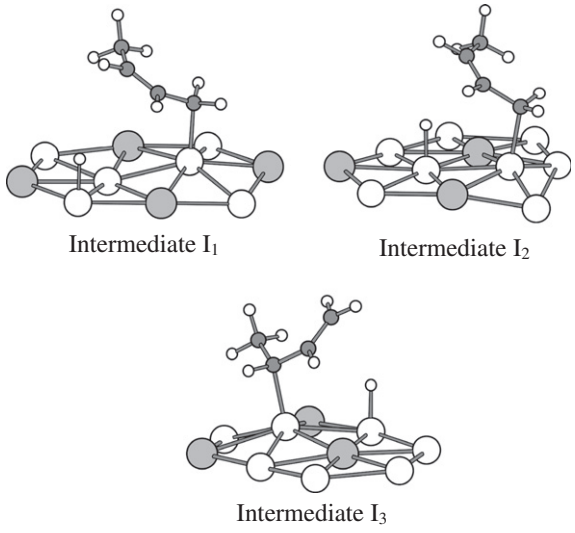

Fig. 9. Optimized geometries of the three intermediates I_1, I_2 and I_3 found during the hydrogenation of 1-buten-3-yl into 1-butene and 2-butene on ($\sqrt{3} \times \sqrt{3}$)R30° Pt_2Sn/Pt(1 1 1).

that the three products should be produced competitively. However, the high barrier of the first step prevents this path to be kinetically relevant. Hence, only the bottom path will be considered further for explaining the selectivity. It immediately appears from Fig. 8 that the pathway leading to 1-butene from 1-buten-3-yl is far less energetic than the two other ones, with an overall barrier of 33 kJ mol^{-1}, although it occurs in several steps. The final result is that 1-butene will be obtained preferentially in agreement with the experimental results. The transition state yielding 2-butene is the second less energetic one (50 kJ mol^{-1}), which explains that 2-butene is also obtained. Nevertheless, the difference with the barrier leading to 1-butene is too large to explain the experimental ratio. A possible reason could be the isomerization of 1-butene into 2-butene as observed experimentally [8,39], likely through a process of dehydrogenation–rehydrogenation steps, the occurrence of which depends on the coverage in hydrogen. The transition state leading to butane-1,3-diyl is much higher in energy, and the metallacycle will not be formed, which is a key point for not obtaining butane as a primary product. Moreover, the previous thermodynamic argument explains why butene is not further hydrogenated to butane. Hence, the calculated pathways and thermodynamics completely explain the high selectivity to butenes observed experimentally on Pt/Sn alloy and the absence of butane as primary product. The rate-limiting step for the formation of 1-butene is the first hydrogenation with a barrier of 71 kJ mol^{-1}, in very good agreement with the experimental activation energy of 72 kJ mol^{-1} determined from temperature-programmed desorption on the Pt_2Sn/Pt(1 1 1) surface alloy [19].

The whole reactivity study has been made on the adsorbed *cis* isomer of butadiene that is the most stable one. Nevertheless, we have tested qualitatively if the *trans* isomer behaves similarly. Effectively, the transition state to obtain the 3-buten-1-yl intermediate has been located at high energy, 122 kJ mol^{-1} above the coadsorbed precursor state. The path leading to 1-buten-3-yl is also a two-step mechanism with decoordination of one double bond, giving a di-σ or π butadiene, only 27–30 kJ mol^{-1} less stable. From the latter, 1-buten-3-yl is obtained with a barrier of 23 kJ mol^{-1}. Hence, the behavior of the *trans* isomer of butadiene is the same as that of the *cis* isomer. Further steps have not been considered so far.

Let us compare now the present results with those obtained for Pt(1 1 1). The situation is totally different [15]. In the Pt case, the two paths leading to 3-buten-1-yl and 1-buten-3-yl have a similar energy barrier (97 kJ mol^{-1}), while on the alloy, the path yielding 3-buten-1-yl requires a much higher barrier (136 kJ mol^{-1}) than the one leading to 1-buten-3-yl (92 kJ mol^{-1}, without decoordination). A first explanation can be the stability difference between these two intermediates on the various metal surfaces. This difference is smaller on Pt(1 1 1) (17 kJ mol^{-1}) than on Pt_2Sn/Pt(1 1 1) (37 kJ mol^{-1}, Table 3). This can be connected to the ability of Pt_2Sn/Pt(1 1 1) to favor the π adsorption mode of alkenes relatively to the di-σ mode (compare the butene adsorption in [15] and in the present work). Following the Hammond principle, the TS leading to 3-buten-1-yl is higher on Pt_2Sn/Pt(1 1 1) than on Pt(1 1 1). Besides, the comparison of the Sn—H distances in the two corresponding transition states TS_2 and TS_1 (Fig. 7) shows that in TS_1, H is closer to Sn than in TS_2 (2.64 vs. 3.02 Å). This is due to the position of the C^2 carbon atom in adsorbed butadiene (Fig. 5) that lies closer to Sn than C^1. Moreover, the structure of TS_2 is more flexible than the one of TS_1 since the attack is at one end of the molecule. Hence, the attacking H passes and stays closer to Sn in TS_1, which is destabilizing as we have observed that hydrogen tends to avoid tin (Section 3.2). Thus, Sn blocks the formation of 3-buten-1-yl and forces the mechanism to pass through the 1-buten-3-yl monohydrogenated intermediate for which the barrier is smaller than on Pt(1 1 1): 92 vs. 97 kJ mol^{-1}. Moreover, the formation of 1-buten-3-yl is even easier (barrier 71 kJ mol^{-1}) than on Pt if the second elementary mechanism, with partial decoordination of butadiene to a di-σ form and attack of H on the decoordinated double bond, is considered. Such a mechanism is also possible on Pt(1 1 1) but

leads to a high-energy TS from a larger cost for the partial butadiene decoordination.

If the second hydrogenation is concerned, there is a competition on Pt(1 1 1) between the formation of 1-butene and butan-1,3-diyl starting from both 3-buten-1-yl and 1-buten-3-yl. In the case of the alloy, the conversion of 1-buten-3-yl to butan-1,3-diyl requires a similar energy to the one calculated on Pt(1 1 1) (92 vs. 99 kJ mol^{-1}). However, the conversion to 1-butene is far less activated (33 kJ mol^{-1}). The reason is that the C=C double bond decoordinates from the surface in a first step. Again, such a decoordination would cost too much energy in the case of Pt.

From these comparisons, one can conclude that the hydrogenation of butadiene on the Pt_2Sn/Pt(1 1 1) alloy surface is different from the reaction on Pt(1 1 1). On the alloy, the hydrogenation through 3-buten-1-yl is not favored, and in the pathway passing through 1-buten-3-yl, the barrier leading to the metallacycle is much higher than the one leading to 1-butene. This explains why the alloy Pt_2Sn/Pt(1 1 1) is totally selective contrarily to Pt(1 1 1).

Except TS_1, TS_4, TS_{12} and TS_{13} that have been discussed above, the other transition states behave similarly on the alloy and on Pt(1 1 1), with activation energies ranging from 70 to 99 kJ mol^{-1} compared to 99–125 kJ mol^{-1} on platinum. In all these cases, the attacking H is nearly atop the involved Pt atom, far from the Sn atoms. The activation barriers are smaller than on Pt(1 1 1) because of the weaker bonds on the alloy between the adsorbed species and the surface. The weakening of the adsorption strength is all the more large as the species create more bonds with the surface. Hence, the transition states are less destabilized on the alloy than the starting points, which reduces the barriers, if no other factor intervenes.

Finally, the role of tin in the enhancement of the selectivity toward 1-butene compared to Pt(1 1 1) is dual. First, by a repulsive effect on H, it helps preventing the hydrogenation from going through 3-buten-1-yl, of which the further hydrogenation is not selective. Secondly and more importantly, by a ligand effect, it allows the easy decoordination of the C=C double bond prior to hydrogenation, hence opening a new low-energy hydrogenation pathway and favoring the formation of 1-buten-3-yl and of 1-butene.

Here, a parallel can be drawn with the case of acrolein hydrogenation at the C=O double bond [41]. In that case indeed, the lowest energy path is also a multistep one. In both cases, there is decoordination of the double bond to be hydrogenated prior to hydrogenation, the molecule remaining bound to the surface through another unsaturated carbon atom. Such a mechanism is possible when the double bond in question is sufficiently weakly bound. This is the case for the C=O bond on Pt(1 1 1) and for the C=C bond on Pt_2Sn/Pt(1 1 1) since it is known that the presence of tin reduces considerably the C=C bond adsorption strength.

The behavior of Pt_2Sn/Pt(1 1 1) can also been compared to that of another catalyst providing a high selectivity to butene, namely palladium. The comparison of the energy profiles obtained in the present study with those obtained for Pd(1 1 1) [15] reveals a great similarity. Indeed, there is the same marked discrimination between the pathways with initial C—H formation at the C^2 or C^1 carbons, in disfavor of the former. Then, the second step starting from 1-buten-3-yl (product of attack at C^1) is clearly selective toward the formation of butene against the formation of butan-1,3-diyl, with a smaller barrier. However, if the energy profiles look similar, the reasons for the improved selectivity for PtSn and Pd, vs. Pt, are different. In the case of Pd(1 1 1), our argumentation to explain the high selectivity rested on the energy difference between the two monohydrogenated intermediates or between the products, inducing a difference in energy barrier from a Brønsted–Evans–Polanyi-type relation [42]. This argument still holds for the first hydrogenation step in the case of Pt_2Sn/Pt(1 1 1), where a significant energy difference exists also between 3-buten-1-yl and 1-buten-3-yl, favoring the attack at C^1. This energy difference could be related to the ability of Pd(1 1 1) and Pt_2Sn/Pt(1 1 1) to favor the π adsorption mode of alkenes relatively to the di-σ mode (See Fig. 5, Table 1 and Ref. [14]), in contrast to Pt(1 1 1). This thermodynamic argument is however not valid at all for the second hydrogenation step on Pt_2Sn/Pt(1 1 1) and the high barrier for butane-1,3-diyl vs. butene formation, since chemisorbed butane-1,3-diyl is only 10 kJ mol^{-1} less stable than 1-butene (this energy difference is 11 kJ mol^{-1} on the non-selective Pt(1 1 1) surface and 40 kJ mol^{-1} on the selective Pd(1 1 1)). The effect of Pt_2Sn/Pt(1 1 1) surface alloy stems from the weakening of the butadiene adsorption, with respect to Pt(1 1 1) and Pd(1 1 1), which favors partial decoordination of butadiene and triggers the C—H bond formation on the non-coordinated C=C bond, hence markedly lowering the barrier for 1-butene or 2-butene formation. Indeed, this non-coordinated pathway is not possible for the second C—H bond formation at C^3, which leads to butane-1,3-diyl, since the carbon framework would be too strained in that case.

5. Conclusion

The thermodynamic and kinetic properties ruling the high selectivity of a Pt/Sn alloy surface toward butadiene hydrogenation have been explored from DFT calculations. An exhaustive study of the adsorption modes of 1,3-butadiene, of 1- and 2-butenes and of the metallacycle isomers on the Pt_2Sn/Pt(1 1 1) surface alloy has been performed, at a low coverage of 1/9 ML. Both the adsorption energies and the stability order change from Pt(1 1 1) to the alloy. For instance, adsorbed *cis*-butadiene becomes more stable than trans-butadiene and the π adsorption mode of cis 2-butene prevails over the di-σ one. Some structures do no longer exist because carbon atoms do not bind favorably on surface tin atoms. The adsorption energies are all markedly smaller than on Pt(1 1 1), as it is generally the case for alkenes on Pt/Sn alloys.

The calculation of the Gibbs free adsorption energy shows that only butadiene is adsorbed on the surface alloy in the experimental conditions (360 K, 15 Torr). Hence, it can be assumed that the formed butene desorbs immediately without being further hydrogenated.

The exploration of all the hydrogenation steps leads to the conclusion that the behavior of the Pt_2Sn/Pt(1 1 1) surface alloy is totally different from the one of Pt(1 1 1). In the case of the alloy, the first hydrogenation at a central carbon is inhibited and only hydrogenation at a terminal carbon can occur, whereas on Pt(1 1 1), they are competitive. Then, among the three possible second hydrogenations, those leading to 1-butene and 2-butene are easier than the one leading to 1-3 metallacycle because of the easy decoordination of the central double bond before hydrogenation, the formation of 1-butene being even more favored.

Therefore, the absence of butane in the reaction products on the alloy can be explained by two reasons, the low desorption temperature of butene on the one hand, which prevents its hydrogenation, and the avoided formation of 1-3 metallacycle that could be hydrogenated to butane on the other hand.

Tin plays a dual role. First, a role of site blocking: since hydrogen tends to avoid the tin atoms, some transition states are distorted, which increases the corresponding energy barriers. Secondly and mainly, its ligand effect on the Pt surface atoms decreases the strength of the Pt—C bonds, which allows the decoordination of the double bond in the intermediates leading to 1- and 2-butenes, reducing the activation barrier.

Hence, the DFT calculations presented in the present work allow the qualitative understanding of the high selectivity of the

Pt_2Sn/Pt(1 1 1) alloy compared to Pt(1 1 1) in the hydrogenation of butadiene into butene. The comparison with Pd(1 1 1) can lead to some suggestions for the design of efficient catalysts. Pure metals would be selective if they have the propensity of adsorbing alkenes in the π mode. Alloys of a noble metal would be efficient if the second element plays a dual role as tin does: a repulsive interaction with carbon and hydrogen atoms, modifying the active surface topology with metallic ensembles, and an electronic effect from its electronegativity assuring an electron transfer toward Pt atoms and a weaker adsorption strength of the C=C double bonds. The weaker coordination allows a partial decoordination of butadiene and an easy C—H bond formation on the non-coordinated C=C bond for pathways leading to butene.

Acknowledgments

The authors thank IDRIS in Orsay (Project 609), CINES in Montpellier and PSMN in Lyon, for CPU time and assistance

References

[1] J. Massardier, J.-C. Bertolini, A. Renouprez, in: Proceedings of the 9th International Congress on Catalysis, Calgary, 1988, p. 1222.
[2] T. Ouchaib, J. Massardier, A. Renouprez, J. Catal. 119 (1989) 517.
[3] C.-M. Pradier, E. Margot, Y. Berthier, J. Oudar 43 (1988) 177.
[4] C. Yoon, M.X. Yang, G.A. Somerjai, Catal. Lett. 46 (1997) 37.
[5] J. Silvestre-Albero, G. Rupprechter, H.-J. Freund, J. Catal. 235 (2005) 52.
[6] S. Katano, H.S. Kato, M. Kawai, K. Domen, J. Phys. Chem. B 107 (2003) 3671.
[7] G. Tourillon, A. Cassuto, Y. Jugnet, J. Massardier, J.-C. Bertolini, J. Chem. Soc. Faraday Trans. 92 (1996) 4835.
[8] J.P. Boitiaux, J. Cosyns, E. Robert, Appl. Catal. 35 (1987) 193.
[9] J. Silvestre-Albero, G. Rupprechter, H.-J. Freund, Chem. Commun. (2006) 80.
[10] D.C. Lee, J.H. Kim, W.J. Kim, J.H. Kang, S.H. Moon, Appl. Catal. A: Gen. 244 (2003) 83.
[11] R. Massard, D. Uzio, C. Thomazeau, C. Pichon, J.-L. Rousset, J.-C. Bertolini, J. Catal. 245 (2007) 133.
[12] P. Sautet, J.-F. Paul, Catal. Lett. 9 (1991) 245.
[13] F. Mittendorfer, C. Thomazeau, P. Raybaud, H. Toulhoat, J. Phys. Chem. B 107 (2003) 12287.
[14] A. Valcarcel, A. Clotet, J.M. Ricart, F. Delbecq, P. Sautet, Surf. Sci. 549 (2004) 121.
[15] A. Valcarcel, A. Clotet, J.M. Ricart, F. Delbecq, P. Sautet, J. Phys. Chem. B 109 (2005) 14175.
[16] S.H. Choi, J. Sung Lee, J. Catal. 193 (2000) 176.
[17] S. Verdier, B. Didillon, S. Morin, D. Uzio, J. Catal. 218 (2003) 288.
[18] Y. Jugnet, R. Sedrati, J.-C. Bertolini, J. Catal. 229 (2005) 252.
[19] H. Zhao, B.E. Koel, J. Catal. 234 (2005) 24.
[20] L. Piccolo, A. Piednoir, J.-C. Bertolini, Surf. Sci. 592 (2005) 169.
[21] G. Kresse, J. Hafner, Phys. Rev. B 47 (1993) 558.
[22] G. Kresse, J. Hafner, Phys. Rev. B 48 (1993) 13115.
[23] G. Kresse, J. Hafner, Phys. Rev. B 49 (1994) 14251.
[24] P. Blöchl, Phys. Rev. B 50 (1994) 17953.
[25] G. Kresse, D. Joubert, Phys. Rev. B 59 (1998) 1758.
[26] J.P. Perdew, Y. Wang, Phys. Rev. B 45 (1992) 13244.
[27] A. Atrei, U. Bardi, J.X. Wu, E. Zanazzi, G. Rovida, Surf. Sci. 290 (1993) 286.
[28] M. Galeotti, A. Atrei, U. Bardi, G. Rovida, M. Torrini, Surf. Sci. 313 (1994) 349.
[29] G. Henkelman, B.P. Uberuaga, H.J. Jonsson, Chem. Phys. 113 (2000) 9901.
[30] D. Loffreda, Surf. Sci. 600 (2006) 2103.
[31] F. Delbecq, P. Sautet, J. Catal. 220 (2003) 115.
[32] H. Zhao, B.E. Koel, Surf. Sci. 572 (2004) 261.
[33] Y.-L. Tsai, B.E. Koel, J. Phys. Chem. B 101 (1997) 2895.
[34] C. Becker, F. Delbecq, J. Breitbach, G. Hamm, D. Franke, K. Wandelt, J. Phys. Chem. B 108 (2004) 18960.
[35] F. Delbecq, F. Vigné, J. Phys. Chem. B 109 (2005) 10797.
[36] F. Delbecq, F. Zaera, J. Am. Chem. Soc. 130 (2008) 14924.
[37] C. Becker, J. Haubrich, K. Wandelt, F. Delbecq, D. Loffreda, P. Sautet, J. Phys. Chem. C Lett. 112 (2008) 14693.
[38] J. Fearon, G.W. Watson, J. Mater. Chem. 16 (2006) 1989.
[39] G.C. Bond, G. Webb, P.B. Wells, J.M. Winterbottom, J. Catal. 1 (1962) 74.
[40] F. Delbecq, D. Loffreda, P. Sautet, J. Phys. Chem. Lett. 1 (2010) 323.
[41] D. Loffreda, F. Delbecq, F. Vigné, P. Sautet, J. Am. Chem. Soc. 128 (2006) 1316.
[42] D. Loffreda, F. Delbecq, F. Vigné, P. Sautet, Angew. Chem. Int. Ed. 48 (2009) 8978.